Letter

Entanglement links and the quasiparticle picture

Silvia N. Santalla,[1] Giovanni Ramírez,[2] Sudipto Singha Roy,[3,4,5] Germán Sierra,[3] and Javier Rodríguez-Laguna[6]

[1]*Departamento de Física and Grupo Interdisciplinar de Sistemas Complejos (GISC), Universidad Carlos III de Madrid, Leganés, Spain*
[2]*Instituto de Investigación, Escuela de Ciencias Físicas y Matemáticas, Universidad de San Carlos de Guatemala, Guatemala, Guatemala*
[3]*Instituto de Física Teórica, UAM-CSIC, Universidad Autónoma de Madrid, Cantoblanco, Madrid, Spain*
[4]*Pitaevskii BEC Center, CNR-INO and Dipartimento di Fisica, Università di Trento, Trento, Italy*
[5]*INFN-TIFPA, Trento Institute for Fundamental Physics and Applications, Trento, Italy*
[6]*Departamento de Física Fundamental, UNED, Madrid, Spain*

(Received 11 August 2022; accepted 17 March 2023; published 29 March 2023)

The time evolution of a quantum state with short-range correlations after a quench to a one-dimensional critical Hamiltonian can be understood using the *quasiparticle picture*, which states that local entanglement spreads as if it was carried by quasiparticles which separate at a fixed speed. We extend the quasiparticle picture using the recently introduced link representation of entanglement, allowing us to apply it to initial states presenting long-range correlations. The entanglement links are current correlators, and therefore follow a wave equation on the appropriate configurational space which allows us to predict the time evolution of the entanglement entropies. Our results are checked numerically for free fermionic chains with different initial entanglement patterns.

DOI: 10.1103/PhysRevB.107.L121114

Link representations of entanglement. Entanglement is a central concept for most recent developments in quantum theory [1]. Let us consider the von Neumann entanglement entropy (EE) $S_A = -\mathrm{Tr}(\rho_A \log \rho_A)$ of a block A, obtained from the reduced density matrix of a pure state, $\rho_A = \mathrm{Tr}_{\bar{A}}|\psi\rangle\langle\psi|$, where $\bar{A}$ is the complement of A. The state is said to follow the area law when $S_A \propto |\partial A|$, i.e., when the EE of a block A is proportional to the measure of its boundary [2,3]. The area law provides a deep connection between entanglement and geometry [4], paving the route for the recent holographic approaches to a quantized gravity [5]. Moreover, it can be generalized into the so-called link representations of entanglement [6], which associate to each pure state on an N-partite system a symmetric matrix J, with $J_{ij} = J_{ji} \geqslant 0$, $1 \leqslant i, j \leqslant N$, whose entries are called the *entanglement links* (ELs), such that

$$S_A = \sum_{i\in A,\, j\in\bar{A}} J_{ij}, \tag{1}$$

for all possible blocks A (see Fig. 1 for an illustration). Since there are 2^N different blocks and the EL matrix only contains $N(N-1)/2$ parameters, we cannot ensure the existence of an exact link representation, except in a few notable cases, such as valence bond states [7]. Yet, approximate link representations with low errors have been found for many relevant states. Interestingly, the entropies built from a link representation fulfill naturally the subadditivity constraints [6].

Within a continuous framework we can write the EL as a two-point function $J(x, y)$, such that

$$S_A = \int_A dx \int_{\bar{A}} dy\, J(x, y). \tag{2}$$

For a one-dimensional (1D) system, this provides an approximate route to find the EL,

$$J(x, y) = \tfrac{1}{2}\partial_x\partial_y S_{[x,y]}, \tag{3}$$

where $S_{[x,y]}$ denotes the EE of the block $[x, y]$. Of course, in a discrete setup the derivatives in Eq. (3) become finite differences,

$$J_{ij} = \tfrac{1}{2}(S_{i,j} - S_{i+1,j} - S_{i,j+1} + S_{i+1,j+1}), \tag{4}$$

where $S_{a,b}$ denotes the EE of $A = \{a, \ldots, b-1\}$. This link representation is exact for compact blocks, losing its accuracy slowly as the number of fragments in the partition is increased. We should stress that the ground states (GSs) of critical systems possess a very clean link representation, with $J(x, y) \approx (c/6)|x - y|^{-2}$, thus showing that Eq. (1) applies to states with a logarithmic violation of the area law [8–10], because their entanglement entropy scales as $S_{[x,y]} \approx (c/3)\log(|x - y|/\varepsilon)$, where ε is the UV cutoff. This scaling suggests that the entanglement links can be associated with the expectation value of current operators,

$$J(x, y) = \langle \mathbf{J}(x)\mathbf{J}(y)\rangle, \tag{5}$$

which is indeed the case if we let $\mathbf{J}(z, \bar{z}) = \mathbf{J}_L(z) + \mathbf{J}_R(\bar{z})$, with [6]

$$\mathbf{J}_L(z) \equiv \lim_{n\to 1^+} \frac{1}{\sqrt{2(1-n)}}\partial_z \mathcal{T}_n(z), \tag{6}$$

where $\mathcal{T}_n(z)$ is the *twist field operator* of order n [10–12], and we define $\mathbf{J}_R(\bar{z})$ as the equivalent antiholomorphic part. The scaling dimension of the twist operators is $\Delta_n = \frac{c}{12}(n - 1/n)$, thus proving that the entanglement current operator $\mathbf{J}(z)$ has scaling dimension 1 and therefore $\partial_{\bar{z}}\mathbf{J}_L(z) = \partial_z\mathbf{J}_R(\bar{z}) = \mathbf{0}$. We are therefore led to claim that

$$\partial_z\partial_{\bar{z}}\mathbf{J} = \mathbf{0}, \tag{7}$$

i.e., the full entanglement current follows a wave equation. The remainder of this Letter is devoted to exploring the consequences of Eq. (7) and providing numerical checks in particular cases.

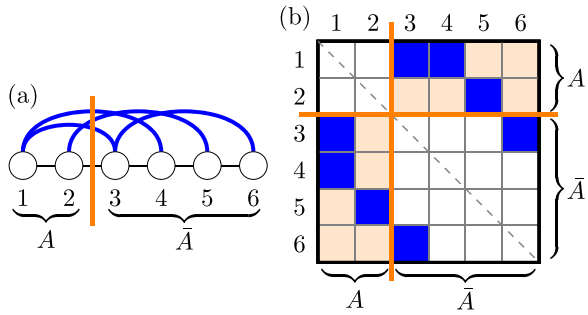

FIG. 1. Illustration of the link representation. (a) Let us consider a quantum state containing $N = 6$ units, whose nonzero entanglement links (ELs) are denoted by the blue arches. The entanglement entropy (EE) between blocks $A = \{1, 2\}$ and $\bar{A} = \{3, 4, 5, 6\}$ can be obtained adding up the values of the nonzero ELs crossing the boundary between them (orange line). (b) The EL can be displayed more clearly in matrix form, and the EE between blocks A and $\bar{A}$ is obtained by adding up the matrix entries in the shaded regions above the diagonal.

Entanglement link dynamics. The quasiparticle picture (QPP) successfully describes the time evolution of the EE when a state with short-range entanglement is quenched to a critical Hamiltonian [13–16]. In this work we extend the quasiparticle picture using the link representation framework, in order to characterize the time evolution of the EE of different initial states, including those presenting long-range entanglement. Our examples include dimerized states [see Fig. 2(a)], the rainbow chain of N sites [17–26], whose GSs can be approximately described as a concentric set of valence bond states between site i and site $N + 1 - i$ [see Fig. 2(b)], or the *bridge state* that we introduce here, which presents bonds between sites i and $i + N/2$, with $i \in \{1, \ldots, N/2\}$ [see Fig. 2(c)].

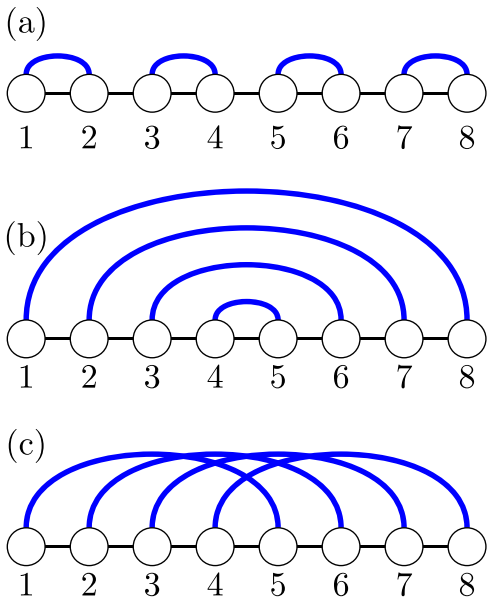

FIG. 2. Illustration of the initial states considered. (a) Dimerized state. (b) Rainbow state. (c) Bridge state.

According to the QPP, when we quench a short-ranged state using a 1D critical Hamiltonian the EE of a block of size $\ell = |x - y|$ at time t behaves approximately as

$$S(\ell, t) = \begin{cases} \sigma v t, & v t < \ell, \\ \sigma \ell, & v t > \ell, \end{cases} \tag{8}$$

where v is twice the speed of light, which may depend on the structure of the initial state [27,28], and $\sigma > 0$ is the EE per site at saturation, and we have neglected the initial value of the EE. This expression can be written alternatively as

$$S(\ell, t) = \sigma v t\, \Theta(\ell - v t) + \sigma \ell\, \Theta(v t - \ell), \tag{9}$$

where $\Theta(x)$ is the Heaviside function. Using Eq. (3) we can estimate the entanglement links,

$$J(\ell, t) = -\frac{1}{2}\partial_\ell^2 S(\ell, t) = \frac{\sigma}{2}\delta(v t - \ell), \tag{10}$$

which represents an *entanglement wave*. Indeed, it is straightforward to check that this expression fulfills the wave equation,

$$\frac{1}{v^2}\partial_t^2 J(\ell, t) = \partial_\ell^2 J(\ell, t), \tag{11}$$

which can be regarded as an extension of the QPP, in accordance with Eq. (7) and the requirements of conformal invariance.

Let us check the validity of Eq. (11) using as our quenching Hamiltonian a free-fermionic chain,

$$H_0 = -\frac{1}{2}\sum_{i=1}^{N} c_i^\dagger c_{i+1} + \text{H.c.}, \tag{12}$$

with either open or periodic boundaries, as required. Notice that the propagation velocity is $v = 2$ in this case, since the Fermi velocity is $v_F = 1$. Meanwhile, our initial states will be chosen as GSs of deformed versions of that Hamiltonian

$$H(\mathbf{g}) = -\sum_{i=1}^{N} g_i\, c_i^\dagger c_{i+1} + \text{H.c.}, \tag{13}$$

where $\mathbf{g} = \{g_i\}$ are the hopping amplitudes, and we assume periodic boundaries. The GSs of Hamiltonian (13) are Slater determinants, whose EE can be found using single-body techniques [29]. The ELs are always numerically estimated using expression (3), which has been shown to provide a good link representation of these states [7].

Let us consider a dimerized initial state, defined by $g_i = [1 + (-1)^i \delta]$, using $\delta = 1/2$ and $N = 128$. Figure 3(a) shows the time evolution of the EE of blocks of different sizes ℓ. We observe that each block saturates at a time proportional to its size, as proposed by the QPP. In Fig. 3(b) we can see the EL matrix of the initial state. The only nonzero ELs are located near the diagonal, $J_{i,i+1} = J_{i+1,i}$. Figure 3(c), on the other hand, provides the EL matrix at time $t = 10$, showing that two wavefronts are traveling in opposite directions from the original diagonal, as proposed in Eq. (11) if the initial velocity, $\partial_t J(\ell, t = 0)$, is zero.

EE of the rainbow state. Let us apply the QPP to states out of its initial range of applicability, such as the GS of the free-fermionic rainbow chain [17–26], which presents long-range

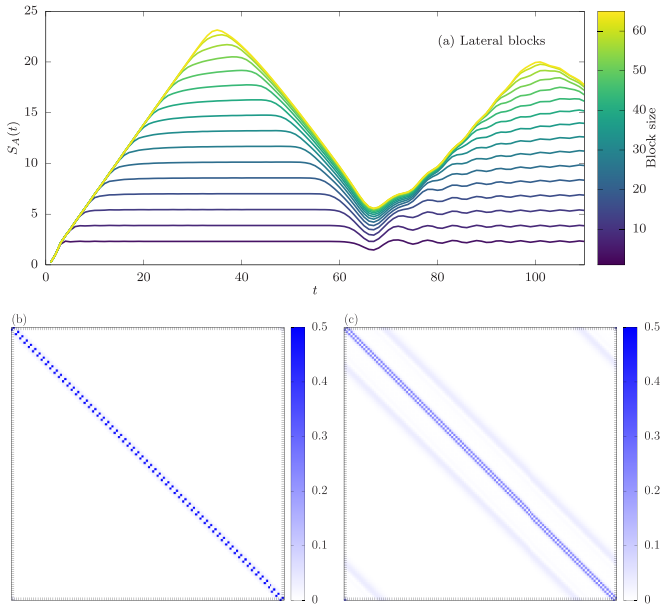

FIG. 3. (a) Time evolution of the EE of the dimerized state with $\delta = 0.5$ and $N = 128$. (b) EL matrix for the dimerized state at time $t = 0$. (c) EL matrix $J(x, y)$ for the dimerized state quenched to the homogeneous Hamiltonian, after a time $t = 10$. Notice the two wavefronts above the main diagonal, traveling in opposite directions, due to the periodic boundary conditions.

entanglement and is defined by Hamiltonian (13) using

$$g_i = \begin{cases} 1 & \text{if } i = N/2, \\ e^{-h(|N/2-i|-1/2)} & \text{otherwise.} \end{cases} \tag{14}$$

The EE of blocks within the GS of the rainbow Hamiltonian grows linearly with their size, $S(\ell) \approx h\ell/6$ for $h \gg 1$, and site i is most strongly correlated to site $N + 1 - i$, thus showing a concentric bond structure which justifies the rainbow term [see Fig. 2(b)]. We will take as our example the case $N = 128$ and $h = 0.7$, which is quenched to the homogeneous Hamiltonian H_0, although in this case we will choose open boundaries. The time evolution of the EE of the lateral blocks $A_\ell = [1, \ldots, \ell]$ is shown in Fig. 4(a). At time $t = 0$ the entanglement entropy of these blocks is proportional to their length, as the volume law requires. The EE of the largest one, $\ell = N/2$, starts to decrease immediately after the quench. Yet, the EE of smaller lateral blocks remains constant for a certain time that increases linearly as the block size decreases. Interestingly, the block of size ℓ starts its decrease when the entropy of all larger blocks reach its starting value. After all the blocks have reached their minimum value they start growing linearly, in similarity to the dimerized state, saturating at a value proportional to their size, corresponding approximately to their initial value.

We may also consider the EE of central blocks of size ℓ, whose initial entanglement is approximately zero, as we can see in Fig. 4(b). They start growing immediately, twice as fast as the lateral blocks decrease.

Extended predictions of the QPP. It is relevant to ask whether the quasiparticle picture can provide an explanation for these observations. Indeed, based on Eq. (7), we propose

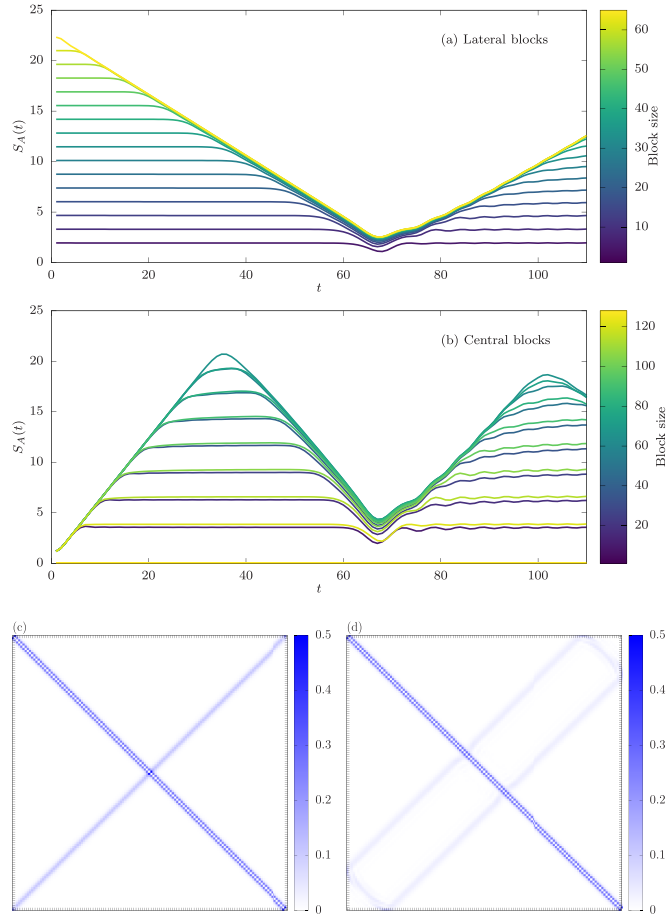

FIG. 4. (a) Time evolution of the EE of lateral blocks within the rainbow state, and (b) same figure for central blocks. (c) EL matrix for the rainbow state at $t = 0$, using $h = 0.7$ and $N = 128$, and (d) EL matrix after $t = 10$, under a quench to an open boundary homogeneous Hamiltonian H_0.

the following wave equation,

$$\frac{1}{v^2}\partial_t^2 J(x, y) = \frac{1}{2}\left(\partial_x^2 + \partial_y^2\right) J(x, y), \tag{15}$$

with suitable boundary conditions, in order to explain the time evolution of both short-ranged and long-ranged initial states. Notice that, due to the symmetry $J(x, y) = J(y, x)$, we could have used only ∂_x^2 or ∂_y^2. Let us apply this equation to the rainbow case, with open boundaries. In Fig. 4(c) we can see the EL matrix for $t = 0$, which contains two different features: a diagonal double line, corresponding to the local entanglement, and an opposite diagonal line, which shows the links between sites i and $N + 1 - i$, which conforms the (approximate) concentric bonds. The time evolution leaves the first line invariant, but it splits the second one into two wavefronts, one of which propagates rightwards and the other one leftwards, as we can see in the EL matrix for $t = 10$ in Fig. 4(d). Moreover, we see a new wavefront appear, parallel to the main diagonal, joining the previous two fronts.

We note that the long-range ELs shown in Figs. 4(c) and 4(d) are solutions of the entanglement wave equation, Eq. (15), if we choose as initial conditions $J(x, y, 0) =$

$\sigma\delta(x+y-N)$ and $\partial_t J(x,y,0)=0$, leading to

$$J(x,y,t)=\frac{\sigma}{2}\delta(x+y-N+vt)+\frac{\sigma}{2}\delta(x+y-N-vt)+\frac{\sigma}{2}\delta(x-y-N+vt), \tag{16}$$

where the last term corresponds to a line parallel to the main diagonal joining the other two lines, due to reflection at the boundaries. Indeed, this is what we can observe to a good accuracy. Yet, the main diagonal of the EL matrix remains static, showing a remanent nonuniversal behavior.

How can we understand Eq. (16) in physical terms? Using Huygens principle, we start out with the rainbow wavefront, which corresponds to the secondary diagonal, $y=N-x$. Each site of the wavefront generates a new circular wave around it, and the new wavefront is given by their envelope. In other terms, each EL *excites* the neighboring links, one slightly stretched, one slightly shrunk, and two slightly displaced leftwards and rightwards. Yet, for the rainbow system the stretched and shrunk links are already excited, so only the translated links appear. Of course, the boundary conditions should also be taken into account: The largest link cannot merely translate, so it gives rise to two links, one in which the left extreme bounces rightwards and another one in which the right extreme bounces leftwards.

Integration of Eq. (16) according to Eq. (2) will provide the time evolution of the EE of any block [30]. Yet, we would like to show a graphical procedure that will yield a better physical intuition in Fig. 5. For the sake of clarity, let us start with an initial state with short-range entanglement, in Fig. 5(a), where we have neglected boundary effects for simplicity. The initial entanglement is denoted by the thick blue line, that splits into two lines traveling in opposite directions. In general terms, the EE obtained when a diagonal line crosses a rectangle is given by the projection of that line on any of the axes. Thus, we see that the EE grows linearly up to time $vt_1=a$, remains constant up to $vt_2=N-a$, and decays linearly down to zero from that moment on [31]. That is the prediction of the QPP, given in Eq. (8).

Let us consider the EL of the rainbow state with open boundaries, schematically drawn in Fig. 5(b) for lateral blocks $A=[0,a]$ with $a<N/2$. Notice that the EE will remain constant up to time $vt_1=N-2a$. Then it will start decreasing linearly until it reaches zero at time $vt=N$. In other terms, we get an expression similar to Eq. (8),

$$S_A(t)=\begin{cases}\sigma a, & vt<vt_1=N-2a,\\ \sigma(a-v(t-t_1)/2), & vt_1<vt<N.\end{cases} \tag{17}$$

Notice that if $a>N/2$, we get the same EE as with the block with size $N-a$. Let us now do the same calculation for central blocks of the form $B=[a,N-a]$, with $a<N/4$, using Fig. 5(c). Notice that the EE starts at zero, grows linearly until time $vt_1=2a$. Then it remains constant until time $vt_2=N-2a$, when it will start a linear decrease to zero at time $vt=N$. In other terms,

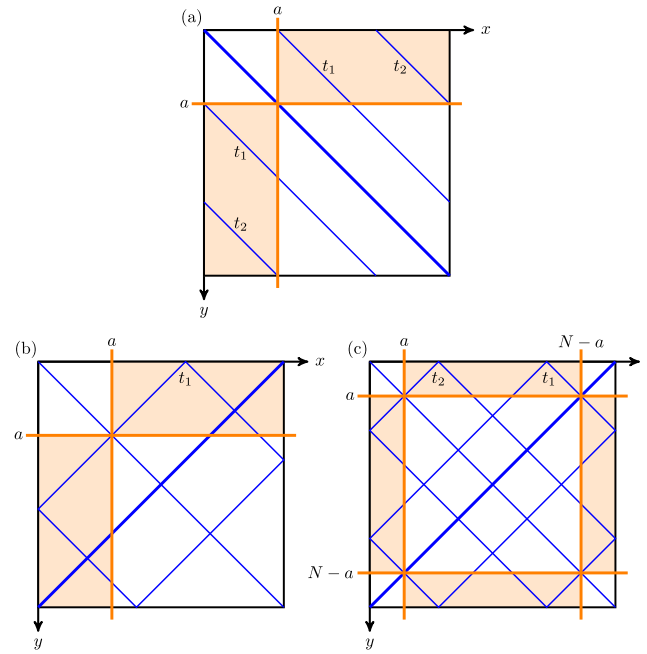

FIG. 5. Illustrating the evaluation of the EE for any time, given the time evolution of the EL. The strong blue line denotes the EL at time $t=0$, and the parallel thin lines correspond to the EL at any later times, traveling with constant speed. (a) Dimerized case. The EE of the block $A=[0,a]$ can be evaluated by counting the EL in the shaded area. Notice that, due to the periodic boundaries, the front is formed by two apparently disjoint segments. (b) Rainbow case, using the same block $A=[0,a]$. (c) Rainbow case, using lateral blocks, $B=[a,N-a]$.

$$S_B(t)=\begin{cases}\sigma vt/2, & vt<vt_1=2a,\\ \sigma a, & vt_1<vt<vt_2=N-2a,\\ \sigma(a-v(t-t_2)/2), & vt_2<vt<N.\end{cases} \tag{18}$$

If $a>N/4$, our graphical procedure shows that the time evolution of the EE of the block $[a,N-a]$ corresponds to that of block $[N/2-a,N/2+a]$, which is approximately the case as we can see in Fig. 4(b).

The persistent subdiagonal. Figures 3(c) and 4(d) show a persistent subdiagonal line in the EL matrix for longer times, which seems to challenge our description. Yet, we should notice that Eq. (15) should be complemented with suitable boundary conditions and probably a source term along the $x=y$ line, which is privileged by the local structure of the quenching Hamiltonian H_0. Thus, we conjecture that the persistent subdiagonal is a nonuniversal phenomenon. Indeed, Fig. 6 shows the behavior of links $J_{i,i+1}$ for the dimerized and rainbow cases analyzed before as a function of time, thus linked to Figs. 3 and 4. In the dimerized case [Fig. 6(a)], the subdiagonal ELs tend to a constant after a quick transient. In the rainbow case [Fig. 6(b)], we observe a wave pulse propagating over a constant background.

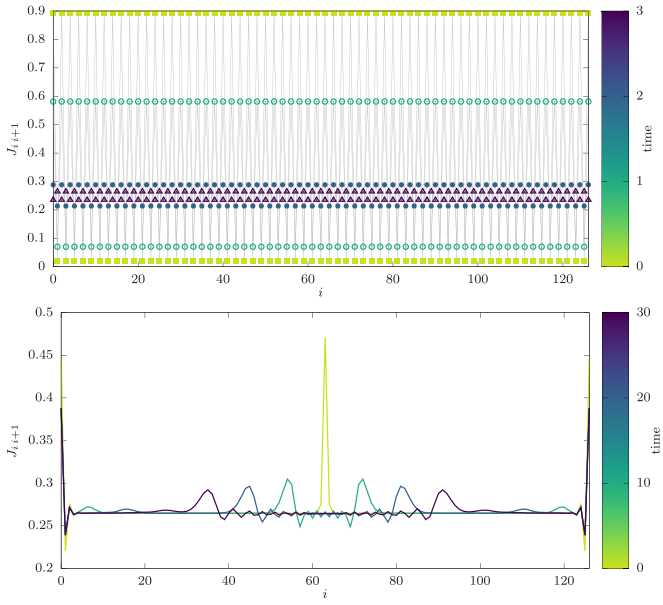

FIG. 6. Subdiagonal ELs of the dimerized and rainbow cases shown in Figs. 3 and 4, as a function of time.

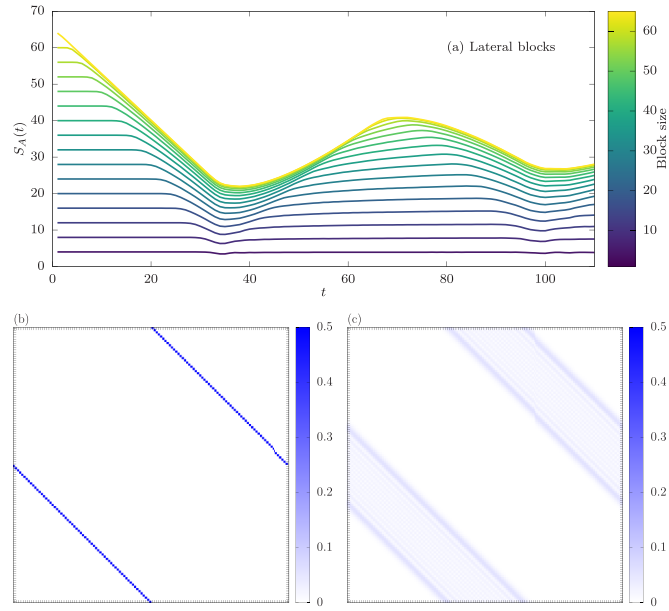

FIG. 7. (a) Time evolution of the EE of contiguous blocks within the bridge state of $N = 128$ sites. Since the state and the quenching Hamiltonian are translation invariant, all contiguous blocks of the same size have the same entropy. (b) EL matrix at time $t = 0$. (c) EL matrix after $t = 10$.

The bridge state. Let us consider one last example, a valence bond state that we will call the *bridge state*,

$$|\Psi\rangle = \prod_{k=1}^{N/2} \frac{1}{\sqrt{2}}\left[c_k^\dagger + (-1)^k c_{k+N/2}^\dagger\right]|0\rangle, \tag{19}$$

where $|0\rangle$ is the Fock vacuum [see Fig. 2(c)]. Now, let us show that the evolution of state $|\Psi\rangle$ after a quench to H_0 (with periodic boundaries) can be described using the extended version of the QPP. At $t = 0$, the state is a valence bond solid, and therefore the EL matrix can be exactly found, $J_{ij} = \sigma\delta_{i,j+N/2 \mod N}$ [7]. We may solve the wave equation with initial condition $J(x, y) = \sigma\delta(x - y + N/2)$ and $\partial_t J(x, y) = 0$, and obtain two traveling waves, $J(x, y, t) = (\sigma/2)\delta(x - y + N/2 + vt) + (\sigma/2)\delta(x - y + N/2 - vt)$, as we can observe in Figs. 7(a) and 7(b). Yet, in this case the wavefronts leave a larger amount of *radiation* behind, since the lattice artifacts are stronger because the initial state is synthetic. We are then led to predict that the entanglement entropy behaves as

$$S(\ell, t) = \begin{cases} \sigma\ell, & vt < N/2 - \ell, \\ \sigma(N/2 - vt), & N/2 - \ell < vt < N/2, \end{cases} \tag{20}$$

before the revivals due to the periodic boundaries, which correspond to the results shown in Fig. 7.

Conclusions and further work. We have extended the quasiparticle picture (QPP) to describe the time evolution of the entanglement entropy after a quench to a critical Hamiltonian, when the initial state presents long-range entanglement. Our extended description of the QPP makes use of the entanglement link (EL) representation for the entanglement entropy of different blocks. Conformal field theory arguments show that the EL must fulfill a wave equation on a tensor-product space built by two copies of the configuration space, due to their nature as current correlators. The propagation velocity associated with the wave equation depends both on the quenching Hamiltonian and the structure of the initial state [27,28], and may even vanish, e.g., in the case of eigenstates of the quenching Hamiltonian. We should stress that our predictions only apply to 1+1D critical Hamiltonians, for any value of their central charge, but they need not apply to noncritical cases, in which another evolution equation should be expected. Moreover, we have observed nonuniversal effects near the diagonal line of the EL matrix, which are in need of further clarification.

Our results have been checked for the case of free fermions on a chain, using initial states with different patterns of entanglement. More numerical experiments are required to check the validity of our formulation for other conformally invariant systems, such as the critical Ising or XXZ models. Moreover, our predictions refer to the EL obtained from the von Neumann entropy. Higher-order Rényi entropies give rise to alternative EL representations which may present a different time evolution and are also interesting to investigate.

Of course, this extension of the QPP is subject to lattice effects which limit its validity in the long run [28,32]. It is relevant to ask how these lattice effects will spoil its predictions for different initial states and different critical models. It is also interesting to wonder about the application of our extension of the QPP to higher-dimensional systems, where we can find phenomena such as the *entanglement tsunami* that describes the evolution of the EE in certain holographic setups [33].

We would like to thank P. Calabrese and E. Tonni for very useful discussions. We acknowledge the Spanish government for financial support through Grants No. PGC2018-095862-B-C21, No. PGC2018-094763-B-I00, No. PID2019-105182GB-I00, No. PID2021-123969NB-I00, No. PID2021-127726NB-I00, No. QUITEMAD+ S2013/ICE-

2801, No. SEV-2016-0597 of the "Centro de Excelencia Severo Ochoa" Programme and the CSIC Research Platform on Quantum Technologies PTI-001. We also acknowledge support by the ERC Starting Grant StrEnQTh (project ID 804305), Provincia Autonoma di Trento, and by Q@TN, the joint laboratory between University of Trento, FBK-Fondazione Bruno Kessler, INFN-National Institute for Nuclear Physics, and CNR-National Research Council.

[1] L. Amico, R. Fazio, A. Osterloh, and V. Vedral, Entanglement in many-body systems, Rev. Mod. Phys. **80**, 517 (2008).
[2] M. Srednicki, Entropy and Area, Phys. Rev. Lett. **71**, 666 (1993).
[3] J. Eisert, M. Cramer, and M. B. Plenio, Colloquium: Area laws for the entanglement entropy, Rev. Mod. Phys. **82**, 277 (2010).
[4] M. M. Wolf, F. Verstraete, M. B. Hastings, and J. I. Cirac, Area Laws in Quantum Systems: Mutual Information and Correlations, Phys. Rev. Lett. **100**, 070502 (2008).
[5] B. Swingle, Entanglement renormalization and holography, Phys. Rev. D **86**, 065007 (2012).
[6] S. Singha Roy, S. N. Santalla, J. Rodríguez-Laguna, and G. Sierra, Entanglement as geometry and flow, Phys. Rev. B **101**, 195134 (2020).
[7] S. Singha Roy, S. N. Santalla, J. Rodríguez-Laguna, and G. Sierra, Link representation of the entanglement entropies for all bipartitions, J. Phys. A: Math. Theor. **54**, 305301 (2021).
[8] C. Holzhey, F. Larsen, and F. Wilczek, Geometric and renormalized entropy in conformal field theory, Nucl. Phys. B **424**, 443 (1994).
[9] G. Vidal, J. I. Latorre, E. Rico, and A. Kitaev, Entanglement in Quantum Critical Phenomena, Phys. Rev. Lett. **90**, 227902 (2003).
[10] P. Calabrese and J. Cardy, Entanglement entropy and quantum field theory, J. Stat. Mech. (2004) P06002.
[11] J. L. Cardy, O. A. Castro-Alvaredo, and B. Doyon, Form factors of branch-point twist fields in quantum integrable models and entanglement entropy, J. Stat. Phys. **130**, 129 (2007).
[12] P. Calabrese and J. Cardy, Entanglement entropy and conformal field theory. J. Phys. A: Math. Theor. **42**, 504005 (2009).
[13] P. Calabrese and J. Cardy, Evolution of entanglement entropy in one-dimensional systems, J. Stat. Mech. (2005) P04010.
[14] P. Calabrese and J. Cardy, Time Dependence of Correlation Functions Following a Quantum Quench, Phys. Rev. Lett. **96**, 136801 (2006).
[15] P. Calabrese and J. Cardy, Entanglement and correlation functions following a local quench: A conformal field theory approach, J. Stat. Mech. (2007) P10004.
[16] M. Fagotti and P. Calabrese, Evolution of entanglement entropy following a quantum quench: Analytic results for the XY chain in a transverse magnetic field, Phys. Rev. A **78**, 010306(R) (2008).
[17] G. Vitagliano, A. Riera, and J. I. Latorre, Volume-law scaling for the entanglement entropy in spin 1/2 chains, New J. Phys. **12**, 113049 (2010).
[18] G. Ramírez, J. Rodríguez-Laguna, and G. Sierra, From conformal to volume-law for the entanglement entropy in exponentially deformed critical spin 1/2 chains, J. Stat. Mech. (2014) P10004.
[19] G. Ramírez, J. Rodríguez-Laguna, and G. Sierra, Entanglement over the rainbow, J. Stat. Mech. (2015) P06002.
[20] J. Rodríguez-Laguna, S. N. Santalla, G. Ramírez, and G. Sierra, Entanglement in correlated random spin chains, RNA folding and kinetic roughening, New J. Phys. **18**, 073025 (2016).
[21] J. Rodríguez-Laguna, J. Dubaîl, G. Ramírez, P. Calabrese, and G. Sierra, More on the rainbow chain: Entanglement, space-time geometry and thermal states, J. Phys. A: Math. Theor. **50**, 164001 (2017).
[22] E. Tonni, J. Rodríguez-Laguna, and G. Sierra, Entanglement Hamiltonian and entanglement contour in inhomogeneous 1D critical systems, J. Stat. Mech. (2018) 043105.
[23] N. S. S. de Buruaga, S. N. Santalla, J. Rodríguez-Laguna, and G. Sierra, Symmetry protected phases in inhomogeneous spin chains, J. Stat. Mech. (2019) 093102.
[24] I. MacCormack, A. Liu, M. Nozaki, and S. Ryu, Holographic duals of inhomogeneous systems: The rainbow chain and the sine-square deformation model, J. Phys. A: Math. Theor. **52**, 505401 (2019).
[25] N. Samos Sáenz de Buruaga, S. N. Santalla, J. Rodríguez-Laguna, and G. Sierra, Piercing the rainbow state: Entanglement on an inhomogeneous spin chain with a defect, Phys. Rev. B **101**, 205121 (2020).
[26] N. Samos Sáenz de Buruaga, S. N. Santalla, J. Rodríguez-Laguna, and G. Sierra, Entanglement in noncritical inhomogeneous quantum chains, Phys. Rev. B **104**, 195147 (2021).
[27] K. Najafi, M. A. Rajabpour, and J. Viti, Light-cone velocities after a global quench in a noninteracting model, Phys. Rev. B **97**, 205103 (2018).
[28] S. Singha Roy, G. Ramírez, S. N. Santalla, G. Sierra, and J. Rodríguez-Laguna, Exotic correlation spread in free-fermionic states with initial patterns, Phys. Rev. B **105**, 214306 (2022).
[29] I. Peschel, Calculation of reduced density matrices from correlation functions, J. Phys. A: Math. Gen. **36**, L205 (2003).
[30] We would like to stress the similarity between Eq. (4.1) of Ref. [13] and the integration of Eq. (16) according to Eq. (2). Indeed, that equation provides a link representation of the time-evolved state within the QPP.
[31] Notice that, due to the periodic boundaries, the wavefront will always be formed by two lines parallel to the main diagonal traveling with opposite velocities. In fact, the two lines in Fig. 5(a) corresponding to times t_1 and t_2 are present at both times, interchanging their velocities in the process. Check Fig. 3(c) where we can see both wavefronts at an early time.
[32] M. Prähofer and H. Spohn, Scale invariance of the PNG droplet and the Airy process, J. Stat. Phys. **108**, 1071 (2002).
[33] H. Liu and S. J. Suh, Entanglement Tsunami: Universal Scaling in Holographic Thermalization, Phys. Rev. Lett. **112**, 011601 (2014).